Structurally complex seagrass obstructs the sixth sense of a specialized avian molluscivore

Jimmy de Fouw, Tjisse van der Heide, Thomas Oudman, Leo R. M. Maas, Theunis Piersma and Jan A. van Gils

ABSTRACT

Predators have evolved many different ways to detect hidden prey by advanced sensory organs. However, in some environmental contexts sensory information may be obscured. The relation between sensory organs, obstruction, and searching efficiency remains little explored. In this study we experimentally examined the ways in which a sensory system ('remote detection'), which enables red knots *Calidris canutus* to detect hard objects buried in wet soft sediments, is obstructed by plants. At an important coastal nonbreeding site of this species, the Banc d'Arguin (Mauritania, West Africa), most of the intertidal foraging area is covered by seagrass. The structurally complex networks of belowground roots and rhizomes and aboveground seagrass may obstruct information on the presence of buried bivalves and thus affect searching efficiency. Under aviary conditions we offered red knots buried bivalves in either bare soft sediments or in seagrass patches and measured prey encounter rates. In seagrass, red knots detected prey by direct touch rather than remotely, the latter which we confirmed they do in bare sediment. Physical modelling of the pressure field build-up around a probing bill showed that within a layer of seagrass rhizomes, permeability is reduced to the extent that the pressure field no longer reveals the presence of an object. In bare sediment, where searching efficiency is constant, red knot intake rate levelled off with increasing prey density (described by a so-called type II functional response). In the seagrass beds, however, prey density increases with seagrass density and simultaneously decreases searching efficiency, which will at some point lead to a decrease in intake rate when prey densities increase (i.e. a type IV functional response).Clearly, prey detection mechanisms dictate that the combined effects of prey density and habitat complexity should be taken into account when predicting forager distributions and habitat preference.

Accepted for publication in *Animal behaviour*

INTRODUCTION

Insights into the morphology and functionality of sensory organs in animals have contributed to our basic understanding of habitat selection and foraging distribution of animals searching for prey (Miller and Surlykke 2001, Sleep and Brigham 2003, Cunningham et al. 2010, Piersma 2012). Predators have evolved multiple ways to detect their prey other than by sight. For example, bats detect their prey in the dark by ultrasonic signalling (Schnitzler and Kalko 2001), owls use high acoustic sensitivity to detect their prey by sound in the dark (Martin 1986) and cetacean species often use echolocation to detect their prey in the water column (Madsen et al. 2004, Au et al. 2007). Using their sensitive bill tip, shorebirds (Scolopacidae) have evolved a variety of ways to detect prey buried out of sight in soft sediments, including smell, taste, detection of prey vibrations, direct touch and even 'remote detection' (Hulscher 1982, Gerritsen and Meiboom 1986, Piersma et al. 1998, Nebel et al. 2005).

In some environmental contexts, sensory information may be obscured. For example, vegetation cover on the water surface obstructs echolocation-based prey detection in insectivorous bats (Boonman et al. 1998), and underwater seagrass meadows may serve as an acoustic refuge for fish from the echolocation sounding by dolphins (Wilson et al. 2013). Yet, the relation between sensory organs, obstruction, and searching efficiency remains rather little explored (Piersma 2011). In this study we experimentally examined whether seagrasses can obstruct prey detection by red knots *Calidris canutus*. Red knots are highly specialized molluscivorous birds that usually forage on bivalves buried in the soft sediments of intertidal mudflats (Piersma 2007, Piersma 2012). Red knots have a sensory organ in the tip of the bill to detect hard-shelled prey buried in soft wet sediments without direct contact (Piersma et al. 1998). As is the case for other shorebirds, the tip of the bill contains numerous tiny pits with clusters of Herbst corpuscles, which in red knots enable the detection of self-induced pressure differences during repeated probing in wet soft sediments. Using this form of 'remote prey detection, red knots detect buried prey faster and more efficiently than if they had to rely on direct touch (Piersma et al. 1995, Piersma et al. 1998). A similar mode of prey detection has been described for kiwis (Apterygidae) and ibises (Threskiornithinae) (Cunningham et al. 2007, Cunningham et al. 2009, Cunningham et al. 2010).

This model of prey detection is applicable to red knots foraging on hard-shelled prey in bare soft sediments (Piersma et al. 1995, van Gils et al. 2006). However, at Banc d'Arguin (Mauritania, West Africa), the subspecies *C. c. canutus* mostly encounters and uses seagrass habitats (Altenburg et al. 1982, van Gils et al. 2015). These habitats consist of structurally complex networks of belowground roots, rhizomes and aboveground leaves (Larkum et al. 2006). We hypothesize that searching efficiency, i.e. the standardized rate at which foragers encounter their prey (Holling 1959), will be negatively influenced by these structures, because the remote detection system requires unobstructed passage of water between the sediment particles (Piersma et al. 1998). To test this idea, we measured searching efficiency in red knots by offering them buried prey either in bare sedi-

ment or in seagrass-covered sediment. Here, the bare sediment treatment served as a control to verify whether red knots where able to find prey remotely (Piersma et al. 1998). Additionally, we developed a model to show the obstructing effect of seagrass rhizomes on the pressure field build-up by the probing bill. We will briefly discuss the implications of this effect on the predicted relationship between prey density and intake rate (i.e. the functional response).

METHODS

Birds

The experiment was conducted in January 2011 at the research station of the Parc National du Banc d'Arguin, Mauritania, West Africa (19°53'N, 16°17'W). Six red knots were caught with mist nets on a nearby shoreline high-tide roost and colour-ringed for individual identification. All birds where successfully released after the experiments. Average bill length was 35.1 mm (range 33.6–37.0 mm) and body mass just after catching was 129 g (range 118–144 g). Birds were kept as a group in a small aviary (2.0 × 0.6 and × 0.4 m high) with sand on the floor, freshwater *ad libitum*, and with local natural day-light cycles and temperatures (varying between 18 and 24°C). Every morning, the birds were weighed and their health status assessed. Birds were fed commercial trout feed (Trouvit; Skretting, Stavanger, Norway) and live bivalves that were collected locally on a daily basis. To keep birds motivated to feed during the trials, daily portions were adjusted to keep body mass just above 100 g (e.g. Oudman et al. 2014, van Gils and Ahmedou Salem 2015).

Experimental design

Feeding trials were conducted in the housing cage, in which a feeding patch (10 cm depth and 15 cm radius) was created with either bare sediment or seagrass (Figure 6.1C-E). *Loripes lucinalis* (8.5–10.5 mm length), the most common bivalve in our study area (Honkoop et al. 2008), was used as prey. Per patch, either 20 or 40 prey items were offered (283 and 566 ind. m^{-2}). All prey were buried at a fixed depth at either 1, 2 or 3 cm. For practical reasons all trials of each combination were offered in the same patch in which prey items were replaced after each trial. All density and depth combinations were offered twice to each bird (although never on the same day). Densities and depth of bivalve prey were well within the range reported for the field (Piersma et al. 1993, van der Geest et al. 2011, van Gils et al. 2013, Ahmedou Salem et al. 2014, van Gils et al. 2015). Patches were filled with sand (mean medium grain size ± SE (n = 6): 248.0 ± 2.7 μm) collected at the nearby intertidal beach (19°53.026'N, 16°17.573'W). Penetrability of the seawater-saturated sand was kept constant by adding seawater till 2 mm of water remained on top of the surface.

Seagrass was collected on a tidal flat (19°53.051'N, 16°17.367'W) 500 m east of the field station. Seagrass densities were within the range reported from the field (range:

2,200–13,000 shoots m^{-2}) (van Lent et al. 1991, Vermaat et al. 1993). A 15-cm high sharpened PVC ring (15 cm radius) was pushed gently into the seagrass (mean shoot density ± SE (n = 5): 8,842 ± 700 m^{-2}). The ring with the seagrass bed was taken out. Metal pins were pushed in horizontally from the side of the ring through the seagrass rhizome mat forming a 2.5 × 2.5 cm mesh holding the seagrass mat intact. Next, the sediment was carefully sieved out, a time-consuming process that was needed to remove all prey living in the seagrass in order to be able to offer precise experimental prey densities. Eventually, a 'clean' intact seagrass mat (rhizomes, roots and leafs) remained in the ring, which was then placed in a 15-cm radius, 10-cm high container, thereafter filled with wet sand, after removing the metal pins. Next, a plastic rod with a scale was used to insert prey in their natural position into the sediment at the aimed depth, at random spatial positions. The hole was filled and the sand was smoothened (Piersma et al. 1995, Piersma et al. 1998).

After a trial ended, the remaining prey items were counted. We never noticed prey movements or any other signs of their presence (i.e. the bivalves showing a siphon or extending a foot). Each trial was conducted with one individual bird at a time, with each bird being involved in at least one trial per day. Within each combination offered on a given day, the order of the birds in the trials was randomly chosen by rolling a dice. The five remaining birds were held in a separated part of the cage such that they were in vocal and visual contact with the experimental bird. A trial stopped after six prey items were encountered or after 15 minutes.

Searching efficiency and touch model

A digital video camera (CANON Powershot G9) recorded each trial. Timing of prey encounters and ingestions were scored digitally with Etholog (Ottoni 2000), and the recordings were played back in slow motion to confirm that we had not missed a prey encounter. In a randomly-searching forager, the interval between two prey encounters, search time (T_s), is inversely related to the product of searching efficiency (a) and current prey density (D; initial prey density minus the number of prey removed (van Gils et al. 2003)):

$$\frac{1}{T_s} = aD \tag{1}$$

which can be rewritten as:

$$log(T_s) = -log(a) - log(D) \tag{2}$$

In this relationship, a slope of -1 indicates random search, while the intercept, –log(a), reflects the negative of searching efficiency (Piersma et al. 1995, van Gils and Piersma 2004). A searching efficiency that does not vary with prey density, together with a handling time that is constant across prey densities, leads to Holling's type II functional response (Holling 1959). In this well-known equation, the intake rate of a forager

increases as a function of prey density, initially at a rate given by searching efficiency until it levels off due to the handling time constraint. Hence, when red knots use remote prey detection the functional response has a steeper slope than in comparison with direct touch (Piersma et al. 1995).

To test to what extent red knots remotely detect buried prey, we compared the experimentally observed searching efficiency with the calculated searching efficiency based on a direct touch model (see for details Hulscher 1982, Zwarts and Blomert 1992, Piersma et al. 1995). We predicted a strong relation with prey depth for the observed searching efficiencies in seagrass, following the touch-model (Piersma et al. 1995). The touch-model was determined with the touch area of the prey (surface projection of prey area), enlarged by the surface area of the bill tip multiplied by the probe rate at each depth (1-cm classes) (Appendix A6) (Zwarts and Blomert 1992). Probe rates were scored during five time intervals (ca.10 s) for a selection of trials (all six birds equally distributed over the two habitat-treatments and three prey depths, n = 36), by slowing down digital video recordings (1/8th of the recording speed). Probe depth was measured five times in each interval by freezing the digital video image at a probe's maximum depth and using an individual's bill length as a reference.

Statistics

Average search- and handling times (each denoted by Y_i) were calculated for every trial, with individual bird as random effect ($bird_i$):

$$log(Y_i) = \alpha + \beta_1\, prey\ depth_i + \beta_2 \log\,(prey\ density_i) + habitat_i + bird_i + \varepsilon_i$$

where $\varepsilon_i \sim N(0, \sigma^2)$.

Search and handling times were log-transformed to meet model assumptions (when Holling's type II functional response holds then the predicted values for β_2 are –1 and 0 for search time and handling time, respectively). We used a one-sample t-test for difference between observed- and the estimated (touch-model) searching efficiency. All statistical analyses were done in R (package *nlme* for mixed-effect models) (R Development Core Team 2014).

The physical model

We developed a physical model to get mechanistic insight into how seagrass may obstruct the remote detection of red knots (for mathematical descriptions see Box 6.1). Observations and experiments by Piersma et al. (1998) showed that knots are able to remotely sense the presence of shells in wet bare sediment, and that their sensory capacity fails in dry but also in very liquid mud. However, a belowground seagrass mat, consisting of a network of roots and rhizomes, reduces the sediment layer's permeability. This may reduce the effective porosity of the soil and obstructs the pressure field build-up by the probing bill of red knots. We will consider first the response to a shell in a mud layer

without rhizomes mat, qualitatively discussed in Piersma et al. (1998). Second, the response to a shell buried in the lower layer containing the rhizomes mat.

The probing of the bill will produce pressure variations in wet sediment (pore-size 180 μm). Red knots rapidly probe in the sediment over a depth of about 0.5 to 1 cm, usually in series of five to 10 probes at a rate of about 6–9 Hz (Piersma et al. 1998). The property of the medium at hand determines in what way it responds to pressure variations. In dry sediments it can either be supported by normal stresses (pressure) in the rigid sediment structure, or be released instantaneously when it surpasses a certain threshold. In fluids, on the other hand, the pressure cannot be built up, as it will immediately respond by means of flows and of waves on the water surface that will quickly remove the added energy towards infinity (see Box 6.1). In wet sediment, however, there is enough water in the pores to produce a flow through it driven by pressure differences. But as the pores are tiny channels whose sides exert a drag on the flow along them, this local increase in pressure needs time to relax and can be maintained for a while, which is the property employed by the birds.

The classical description of flow through wet sediment is one in which the pressure gradient is balanced by friction, proportional to the flow velocity. Because of the complexity of the sand skeleton this is necessarily an empirical relation, known as Darcy's law (e.g. Sleath 1984). Since the fluid is nearly incompressible, this implies the pressure field is governed by a Poisson equation (Lamb 1932) (see for details Box 6.1).

The knot's sense of remote prey detection involves repetitive, shallow probing, followed by a single deep probe in another direction, apparently used to build up of residual pressure near the bill tip. Very likely, compaction is of dominating influence. This refers to the continuous increase in residual pore pressure, owing to the ‘shaking’ of the muddy sand by the probing action of the bill, which may lead to a (local) compaction of sediment due to a rearrangement of sand grains in closer packing and an associated increase in pore pressure. This process plays a dominant role in liquefaction and the formation of quick sand (Sleath 1984). For red knots, the important aspects of this are that also the residual (i.e. time-averaged) pressure pattern is affected by the presence of a shell and that this pattern becomes increasingly `visible' due to its increase at each successive cycle of the probing motion. Together with the directionality offered by the set of pressure sensors (Herbst corpuscles), present over the whole circumference of the bill, this should offer the knot the ability to sense both prey direction and distance (for details see Box 6.1).

For red knots, when foraging in seagrass, however, the permeability of the lower rhizomes layer will be less than that of the upper mud layer. This is due to the decrease in the effective porosity of the sediment. We will assume that the rhizome root structure is so small that we can represent its presence in the form of a reduced effective permeability which will affect the radial pressure distribution discussed above. For simplicity, we assume the permeability to be constant within the rhizome layer. Hence the pressure will again be inversely proportional to radial distance, but with reduced ‘transmitted’ amplitude. In fact, the semi-permeable interface between the mud and rhizome layers acts as a partial mirror. This will result in an augmented pressure field in the upper sediment layer.

Ethical note

All possible efforts were made to minimize physical and mental impact on the experimental animals. Each bird was weighed and visually inspected for general condition daily. All experimental animals were released in the wild in healthy condition after the experiment with an average body mass of 147 g (range 136–160 g) after two days of *ad libitum* food. The experiment was performed under full permission by the authorities of the PNBA. No animal experimentation ethics guidelines exist in Mauritania but the experiments were performed in accordance with Dutch animal experimentation guidelines. The NIOZ Royal Netherlands Institute for Sea Research has been licensed by the Dutch Ministry of Health to perform animal experiments under licence number 80200.

RESULTS

Searching efficiency and Holling's type II functional response

Search time decreased with increasing prey density with an estimated slope –0.947 (95% confidence interval: lower –1.172; upper –0.722) which did not differ from –1 (i.e. random search), showing that searching efficiency was independent of prey density (Table 6.1). Likewise, handling time was independent of prey density (Table 6.1). Thus, both assumptions of Holling's type II equation were met. Searching efficiency differed significantly between bare sediment and seagrass and decreased with depth (Table 6.1) in both habitat treatments, with the decrease being stronger in seagrass than in bare sediment (significant interaction between depth and habitat treatments: Table 6.1, Figure 6.1A). Handling time increased significantly with prey depth in both habitat treatments and was higher in the seagrass (1.01 ± 0.05 s; mean ± SE) than in the bare patches (0.82 ± 0.05 s) (Table 6.1, Figure 6.1B).

Touch-model

There was a significant effect of depth on the probe rate (Table 6.2), but no an effect of habitat treatment (bare sediment versus seagrass) or of prey density (Table 6.2). In bare sediment, there was a significant difference between the predicted searching efficiency based on the touch model and the observations (Figure 6.1A; at 1 cm: $\text{difference}_{\text{obs-pred}} = -1.58$ cm^2 s^{-1}, $t_{23} = -2.98$, $P < 0.01$; at 2 cm: 4.30 cm^2 s^{-1} $t_{24} = 5.98$, $P < 0.001$; at 3 cm: 3.52 cm^2 s^{-1}, $t_{23} = 11.22$, $P < 0.001$). In seagrass, however, the predicted searching efficiency based on a touch-model did not differ from the observations when prey were buried at greater depths (Figure 6.1A; at 1 cm: $\text{difference}_{\text{obs-pred}} = -3.78$ cm^2 s^{-1}, $t_{23} = -5.31$, $P < 0.001$; at 2 cm: –0.16 cm^2 s^{-1}; $t_{22} = -1.53$, $P = 0.14$; at 3 cm: 0.11 cm^2 s^{-1}, $t_{24} = -0.84$, $P = 0.41$) (observed estimates: bias-corrected back-transformed; Sprugel 1983). This implies that red knots were unable to use remote detection when foraging in seagrass.

Table 6.1 Mixed-effect model of the log-transformed search time, searching efficiency and handling time. Models include fixed effects prey depth (continuous), prey density (continuous), habitat (categorical; seagrass or bare sediment) and individual bird as random effect.

Search time (s)	**Estimate**	**SE**	***t***	***P***
Fixed effects				
Intercept	−0.983	0.172	−5.725	<0.0001
prey depth (1, 2, 3 cm)	0.135	0.030	4.535	<0.0001
habitat (seagrass)	−0.024	0.091	−0.261	0.773
prey density	−0.945	0.114	−8.320	<0.0001
habitat × prey depth	0.170	0.042	4.053	<0.001
Random effects				
Individual bird	1.20×10^{-5} (sd)			
Residual	0.202 (sd)			

Searching efficiency ($cm^2\ s^{-1}$)	**Estimate**	**SE**	***t***	***P***
Fixed effects				
Intercept	1.111	0.065	16.961	<0.0001
prey depth (1, 2, 3 cm)	−0.135	0.030	−4.517	<0.0001
habitat (seagrass)	0.026	0.091	0.290	0.773
habitat × prey depth	−0.172	0.042	−4.061	<0.001
Random effects				
Individual bird	0.015 (sd)			
Residual	0.209 (sd)			

Handling time (s)	**Estimate**	**SE**	***t***	***P***
Fixed effects				
Intercept	−0.351	0.065	−5.388	<0.0001
prey depth (1, 2, 3 cm)	0.095	0.016	5.872	<0.0001
habitat (seagrass)	0.097	0.049	1.984	<0.05
prey density	−0.001	0.001	−1.373	0.172
habitat × prey depth	0.001	0.022	0.011	0.992
Random effects				
Individual bird	0.135 (sd)			
Residual	0.111 (sd)			

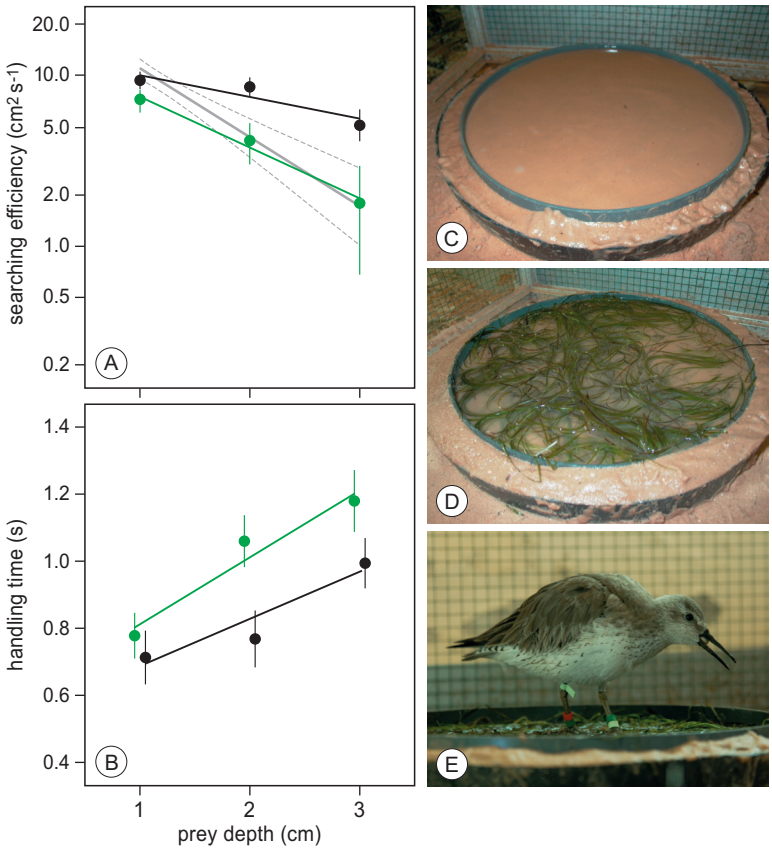

Figure 6.1 (A) Searching efficiency as a function of prey depth of knots foraging on prey in bare (black) and seagrass (green) habitat. The grey lines indicate the touch-model with confidence interval (95%). (B) Prey handling time as a function of prey depth of knots foraging on prey in bare (black) and seagrass (green) habitat. (C) Bare patch, (D) seagrass patch, (E) knot swallowing a prey during an experimental trial on a seagrass patch.

The physical model

The physical model shows that the pressure patterns produced by the probing knot's bill, located at the interface between air and sediment, and the flow through the pores, driven by pressure differences, is influenced by the presence of a spherical shell deeper in the sediment (Figure 6.2A). The imposed pressure gradient is displayed by a spherically symmetric radial decay decreasing from high pressure to low pressure. The isobars are obstructed in the vicinity of the shell (Figure 6.2A). The pressure pattern induced by the presence of the shell is defined by subtracting the response of the initial pulse with the spherical shell in place and without the shell in place. It is this difference that we argue is sensed and informs the knot about the presence of a prey, at some radial distance and direction (Figure 6.2B). When the spherical shell is situated within an infinite rhizomes

layer, which reduces the permeability, the rhizomes layer changes the apparent strength of the source at the origin. The change in the pressure field at the interface between wet sediment and rhizomes layer is clearly visible in a changing isobar inclination (Figure 6.2C). When we again subtract the response pulse with the spherical shell in place and without the shell in place, it shows that the pressure field no longer reveals the presence of the shell. The pressure difference is very nearly symmetric at the bill tip, at the origin, and no longer offers any clues on the direction (nor distance) at which the prey can be found (Figure 6.2D).

Table 6.2 Mixed-effect model of probe rat, with fixed effects prey depth (continuous), prey density (continuous), habitat (categorical; seagrass or bare sediment) and individual bird as random effect.

Probe rate (s^{-1})	**Estimate**	**SE**	***t***	***P***
Fixed effects				
Intercept	15.277	1.401	10.882	<0.0001
prey depth (1, 2, 3 cm)	-4.977	0.397	-12.548	<0.0001
habitat (seagrass)	1.562	0.916	1.705	0.1
prey density	-0.032	0.049	-0.654	0.512
Random effects				
Individual bird	1.062 (sd)			
Residual	1.946 (sd)			

DISCUSSION

Searching efficiency of red knots foraging in seagrass was much lower than when foraging in bare sediment, especially for prey buried at greater depths, and was better explained by the touch model than by remote detection (Figure 6.1A). The present estimates of searching efficiency on bare sediment were similar to previous estimates (5.8 – 26.2 cm^2 s^{-1}) (Piersma et al. 1995, van Gils and Piersma 2004). Nevertheless, we found a small negative effect of depth in bare sediment, an effect not found by Piersma et al. (1995). However, as searching efficiencies in bare sediment were higher than predicted by the touch model, and were quantitatively in line with previous estimates, we conclude that red knots used remote prey detection in bare sediment at all depths (Figure 6.1A). Our finding of the low searching efficiencies (even lower than in the direct touch model) at the shallower prey depths (Figure 6.1A) is probably the result of invisible prey rejections below ground. Searching efficiency is derived from number of prey encountered, so that when prey are detected but rejected below ground without being noticed by the observer, searching efficiency will be underestimated (Wanink and Zwarts 1985, Piersma et al. 1995, van Gils et al. 2015). This bias is likely to become more systematic at high

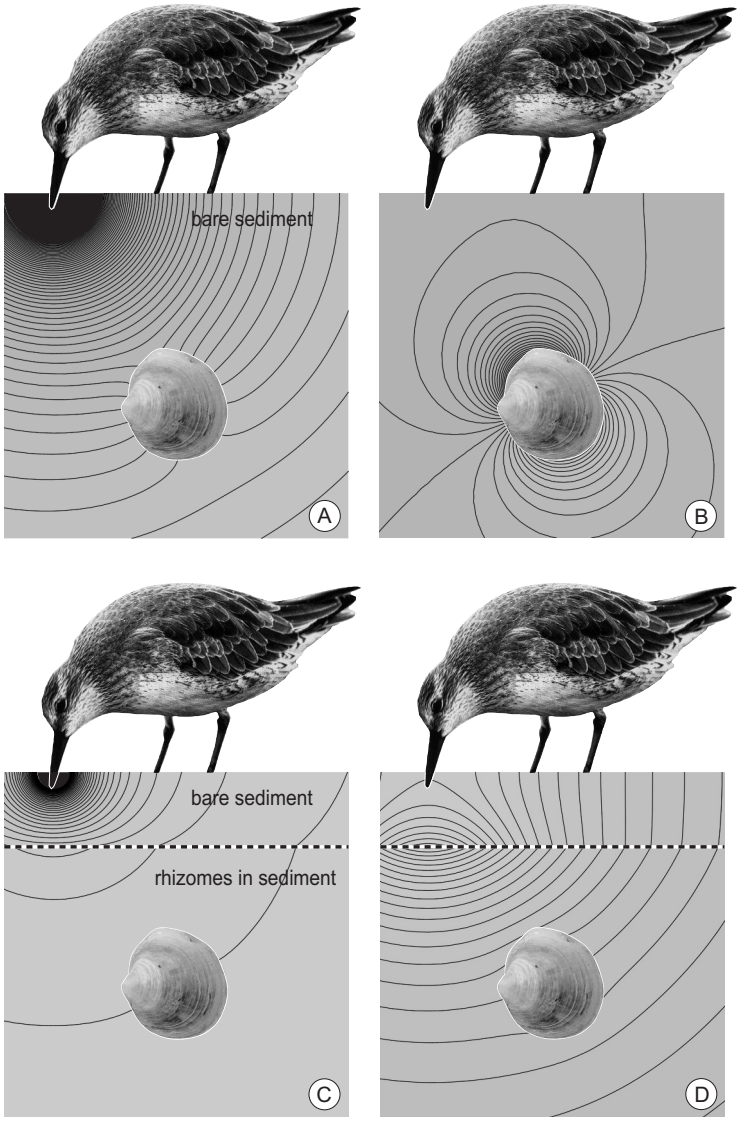

Figure 6.2 (A) The pressure field build-up by the bill of the knot in bare wet sediment of a hypothetical mudflat. The imposed pressure gradient is displayed by a spherically symmetric radial decay decreasing from high pressure (densely packed isobars near bill tip) to low pressure (wider spaced isobars to right). (B) The isobars are obstructed in the vicinity of the shell, and the disturbance pressure field (shown here) is sensed and informs the knot about the presence of a prey, in the form of radial distance and direction. (C) When the spherical shell is situated within an infinite rhizome layer (below the interface between bare wet sediment and infinitely deep rhizome layer, dashed line), which reduces the permeability, the rhizome layer changes the apparent strength of the source at the origin. The change in the pressure field at the interface between wet sediment and rhizomes= layer is visualized by a changing isobar inclination. (D) Here, the pressure difference is nearly symmetric at the bill tip, at the origin, and no longer offers any clues on the direction (or distance) at which the prey can be found (for details see Box 6.1).

prey densities or at shallow depths when prey are more easily found (Wanink and Zwarts 1985; T. Piersma, personal observation).

Handling time increased with prey depth and was higher in seagrass, an effect which was also found by Piersma et al. (1995). In addition, handling time increased more strongly with depth in seagrass which may well be caused by the difficulty for red knots of pulling a prey out of a dense network of rhizomes. The average handling time was 0.92 $\pm$ 0.04 s, which is close to a mean handling time of 0.7 s measured in the field (van Gils et al. 2015).

Why do red knots lose their ability to remotely detect hard-shelled prey when foraging in seagrass? The outcome of the physical model shows that when the spherical shell is situated within a layer of rhizomes, the permeability of this substrate is reduced; the pressure field is changed at the interface between the sediment and the rhizomes (Figure 6.2C). This overwhelms the much weaker pressure difference due to the reflection by the shell and obscures the directional prey information. Therefore, red knots can no longer rely on their remote detection to encounter the hard-shelled prey 'hidden' by the rhizome layer. It also falsely suggests the presence of a prey item at a certain distance right below the bill tip. This indicates that, relative to the vertical, the angular spread of successful deep probes of knots feeding over a rhizome mat should be significantly less than that over a mud layer without a rhizome mat, a hypothesis that deserves testing in future work (see a detailed discussion on the sensitivity of the pressure gradient to the permeability in Box 6.1). All of the pressure differences, of course, also depend on the actual change in permeability due to the rhizomes mat, on the location of that layer and on its depth (here assumed to be of infinite extent). But the dramatic change in the pressure difference that we see because of the rhizome layer (compare Figure 6.2B and 2D) will not depend too much on these details.

Implications for predictions on intake rates and habitat use

Insights into nonvisual sensory systems may give tantalizing opportunities to actually predict habitat selection rules and even foraging distributions (van Gils et al. 2006, Cunningham et al. 2010, Piersma 2011, Piersma 2012). In this study, the remote detection ability of red knots was obstructed by seagrass resulting in decreased searching efficiencies, an important parameter to predict intake rates with a functional response. The functional response is a commonly accepted function to predict spatial distributions and habitat use of foragers (Stephens and Krebs 1986, Piersma et al. 1995, van Gils et al. 2015). However, in bare sediment, where searching efficiency is a constant, red knots obey the assumptions of Holling's type II functional response, implying that intake rate in relation to prey density levels off at high prey densities (this study, Holling 1959, Piersma et al. 1995). Based on our experimental- and physical model results we will argue below that in seagrass beds the relation between intake rate and prey density will be dome-shaped (so called type IV functional response; Holling 1961, Jeschke and Tollrian 2007), implying that above a certain prey density, the intake rate goes down with increasing prey density.

It is known that seagrass has a positive effect on prey density and abundance (Orth et al. 1984, Honkoop et al. 2008, van Gils et al. 2015). In Banc d'Arguin, seagrass and lucinid bivalve densities are tightly linked due to their mutualistic relationship (van der Heide et al. 2012). While at first sight the increase in prey density would be an advantage for knots, 'simultaneously' increasing seagrass density leads to decreasing searching efficiency (Figure 6.3A). Hence, with an increasing seagrass biomass, the searching efficiency decreases faster than the increase in prey densities, so that the functional response will become dome-shaped, and this goes for all depth distributions (Figure 6.3B) (see mathematical details in Appendix A6).

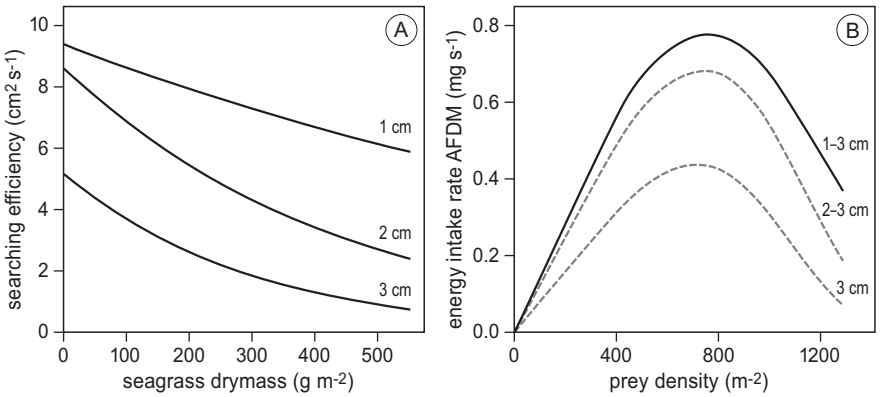

Figure 6.3 (A) Observed searching efficiency versus seagrass density based on experimental results at different prey depths. (B) The predicted functional responses by red knots, cumulative across all prey depths within the experiments (1–3 cm), and cumulative across the two deepest layers (2–3 cm) and for the deepest layer (3 cm). Depth-specific prey density fractions from the field were adapted from Piersma et al. (1993). The horizontal line boxplot shows the median value, the bottom and top of the box show the 25th and 75th percentiles (middle 50% of the data), respectively, whiskers show 1.5 times the interquartile range of the data.

Thus, on the Banc d'Arguin, red knots encounter high searching efficiencies at low prey densities in little or no seagrass, and low searching efficiencies with high prey densities in dense seagrass beds. This shows that in seagrass habitats knots may maximize intake rates by feeding on intermediate prey densities and moderately dense seagrass beds (which is indeed what has been found by van Gils et al. 2015). In other words, in this case the functional response may not be a simple function of prey density but also of seagrass density. Note that in herbivores a type IV response is commonly observed, often because digestive quality decreases with increasing biomass (Fryxell 1991, Heuermann et al. 2011). However, in predator-prey interactions a type IV functional response has not received much attention. Only a handful of recent studies have shown that density-dependent defences, and nutritional quality of the prey, lead to a decline in intake rate at high prey densities (Vucic-Pestic et al. 2010, Bressendorff and Toft 2011, Liznarova and

Pekar 2013, Bijleveld et al. 2016), again suggesting that in many foraging contexts animals should aggregate at intermediate prey densities.

In the Wadden Sea, spatial prediction of foraging red knots was better with than without the refinement of the functional response based on remote (Piersma et al. 1995). In seagrass beds, when seagrass-dependent searching efficiency is not taken into account this may lead to an overestimation of intake rates at high prey densities. The notion of a seagrass-dependent searching efficiency offers a quantitative working hypothesis for future research in diet and habitat preference of red knots foraging on seagrass-covered ecosystems.

ACKNOWLEDGMENTS

We thank the staff of the Parc National du Banc d'Arguin (PNBA) for their permission to work and use their facilities in the park. We especially thank Lemhaba Ould Yarba, Mohamed Ahmed Sidi Cheikh and the local crew at Iwik station: Amadou Abderahmane Sall, Mohamed Camara, Hacen Ould Mohamed Abd, M'Bareck Ould Sangué and Sidi Ould Ely. We thank Bernard Spaans for catching birds, Jeroen Onrust, Mohamed Vall A. Salem and Laura L. Govers for field assistance and the latter also for advice on seagrass collection. Dick Visser prepared the final figures. Two anonymous referees gave helpful comments on the manuscript. This work was largely supported by an NWO-VIDI grant (no. 864.09.002) to J.A.v.G, but also by an NWO-WOTRO Integrated Programme grant (W.01.65.221.00) to T.P., and an NWO-VENI (no. 863.12.003) to T.v.d.H.

APPENDIX A6

Determination of the effective touch area of the prey

To calculate the *effective* touch area we need to determine the touch area of the prey, because the probability of prey being touched depends on the surface area of the prey, measured in the horizontal plane (Zwarts and Blomert 1992). The touch area, determined from digital pictures of *Loripes*, is an allometric function of shell length (n = 27; see inset of *Loripes* touch area, Figure A6.1A) and was analyzed with a nonlinear model based on least-squares estimates (function nls) (Figure A6.1). Red knots probe with a slightly opened bill, apparently to increase the effective touch area (Zwarts and Blomert 1992, Piersma et al. 1998). Therefore, the touch area is enlarged by the average surface area of the bill tip of the red knot, with: t (thickness of bill) = 0.3 cm and w (width of bill) = 0.7 cm (bill parameters taken from: Zwarts and Blomert 1992). The effective touch area is written as: $wt + 2wr + 2tr + \pi r^2$, with r derived from the average touch area from this study based on the allometric function with average prey length of 0.9 cm used in the experiment, see Zwarts and Blomert (1992) for details. Finally, the effective searching efficiency ('touch model') was calculated by multiplying the effective touch area by the effective probe rate at each depth (1-cm classes) (Figure A6.1B).

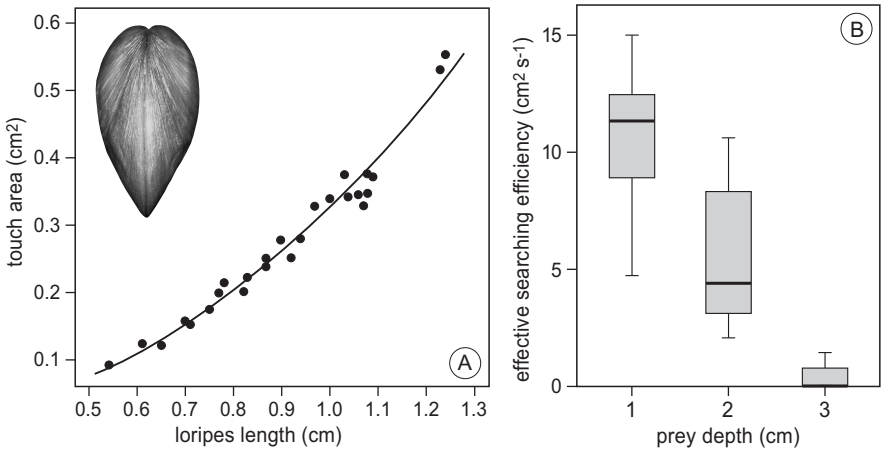

Figure A6.1 (A) Touch area as a function of shell length: $10^a \times L^b$. (a = –0.486 ± SE 0.006, t = –84.36, $P < 0.001$, b = 2.145 ± 0.083, t = 25.88, $P < 0.001$). Average shell length L in the experiments was 0.9 cm. (B) Estimated searching efficiency based on the touch-model.

Functional response

To investigate how searching efficiency affects intake rates (IR) of knots, we integrated the seagrass density dependent searching efficiency into the type II functional response where h is the constant handling time of the prey (s), a is the constant searching efficiency (m^{-2} s^{-1}) and D is the prey density (no. m^{-2}):

$$IR = \frac{aD}{1 + aDh}$$

Because searching efficiency is negatively dependent on seagrass density and decreases with prey depth (Figure 6.3A) and prey density increases with seagrass density, we introduced a dynamic searching efficiency $A(S)$ that is negatively related to seagrass density S:

$$IR = \frac{A(S)D(S)}{1 + A(S)D(S)h}$$

We described the relation between searching efficiency and prey density by the exponential function $A(S) = A(S{=}0)\ e^{-cS}$, where the constant c and $A(S{=}0)$ (the searching efficiency on bare sediment) are fitted to the results of this study. Because the detectability of the prey is depth-dependent, all parameters were estimated for all three depth classes separately by a nonlinear model based on least-squares estimates (function *nls* in R, Figure 6.3A) (R Development Core Team 2014). The relationship between prey density and seagrass biomass was recently quantified non-linearly dependent on seagrass ($D(S)= 256.6\ ^{S}0.24$; chapter 6). We use depth-specific prey density fractions from the field (based on: Piersma et al. 1993) and average energy content of the most common bivalve species, *Loripes* and *Dosinia isocardia*: 7.28 and 2.57 mg $AFDM_{flesh}$ (van Gils et al. 2012). The estimated amount of energy gained based on the functional response becomes dome-shaped and the effect becomes stronger with prey depth (Figure 6.3B).

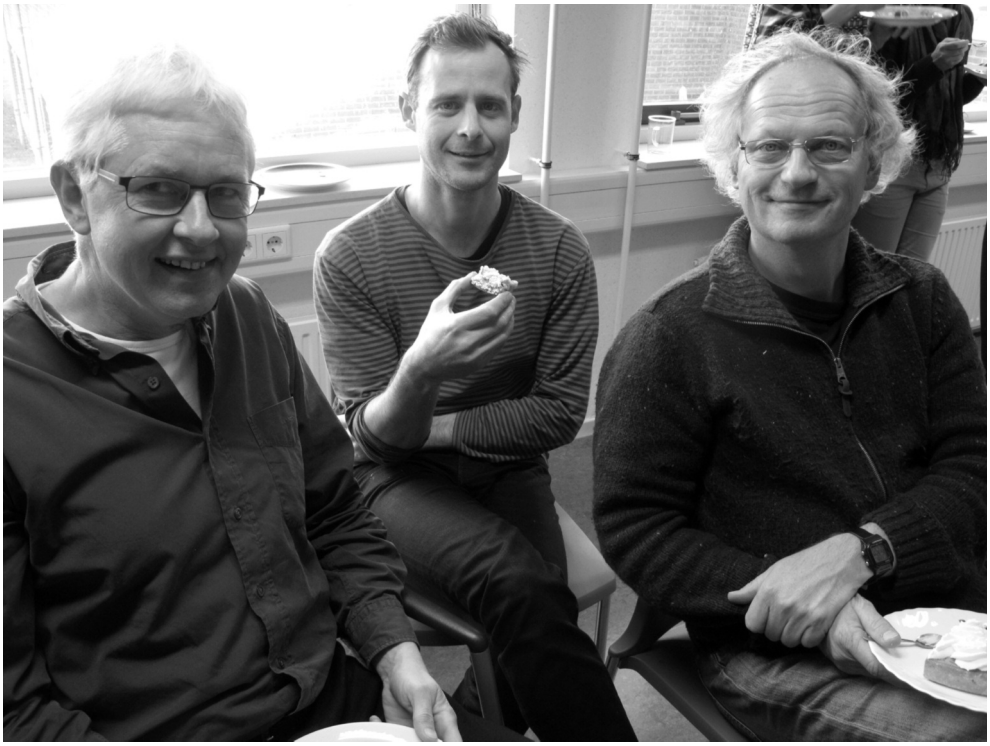

In the 1990s two young passionate scientists joined forces to get insight in a spectacular 'sixth-sense' organ in the tip of the bill of red knots *Calidris canutus* (Piersma et al. 1998). Now, 18 years after date, new insights in the foraging behaviour of red knots forced another young scientist to bring back together these scientists again.

Physical mechanism of remote touch

Leo R.M. Maas, Jimmy de Fouw and Theunis Piersma

ABSTRACT

A simplified physical and mathematical description is given of the mechanism employed by knots for remote detection of shells buried in soft sediments. This mechanism, which employs soil mechanical properties of wet sand, is described both for cases with or without a rhizome (sea grass root) layer below a surface mud layer. The presence of a rhizome layer reduces the permeability of that layer and consequently the knot's remote detection is.

Accepted for publication in *Animal Behaviour* as appendix

INTRODUCTION

Observation and experiments by Piersma et al. (1998) show that knots are able to sense the remote presence of shells (or pebbles), of some 1 cm diameter, in muddy sand. Knots can sense hard-shelled objects, buried over distances up to their bill length (approximately 3 cm). It is significant that their sensory capability fails in dry sand, in very liquid mud and, what is of particular interest here, when there is a rhizome mat shielding their prey (see main text for description).

Observation also shows that the tip of the knot's bill is (uniformly) covered with many tiny pressure sensors (Herbst corpuscles), whose threshold sensitivity (the minimally detectable pressure perturbation) and response time are unknown. We make a few assumptions concerning the bill that will be convenient in its physical modelling. We assume that the probing depth is very small, so that the probe, in its 'emitting' (forcing) mode, acts as a point-source of pressure fluctuations (located at the surface). This is also an accurate description when the emission is produced by a finite-sized spherical object, as long as the same mass-flux is affected. For the conical shape of the bill this should be modified at a later stage. During its detection mode, we assume that the bill penetrates to its true depth.

We first address, the following questions related to the pressure detection mechanism of probing bills and the specific demands posed on the mud and hydrodynamic environment, (1) What is the role of fluid in the mud, and why does the detection mechanism fail in dry or very liquid circumstances? (2) What is the role of the repetitive character of the probing? (Why is a single probe not sufficient?) (3) What is the role of the rhizomes layer on the detection mechanism?

Role of fluid in the mud layer

The probing of the bill will produce pressure variations in the mud. The properties of the medium at hand determine in what way it responds to pressure variations. In dry sandy sediments, for instance, pressure perturbations can, to a large extent, simply be supported by increased or decreased normal stresses of one sand grain upon another, without the necessity of having to yield. In other words, for tiny pressure perturbations, the sand, except in the very vicinity of the bill, acts as a solid. Fluids, on the other hand are unable to support pressure differences and always have to 'yield'. Consequently, they will immediately start to flow, thereby relaxing the pressure difference. Moreover, when forcing is at a liquid surface, the fluid will also respond by means of waves on that surface that will quickly remove the added energy towards infinity. In a muddy environment, however, there is enough water in the pores to produce a flow through it, while the absence of a free, liquid surface, eliminates the ability to remove energy by means of surface wave propagation. The pressure perturbation generated is, in other words, *trapped* in the forcing location.

The flow through pores is driven by pressure differences. The pores are tiny channels whose sides exert a drag on the flow along them. Indeed, side wall friction is the dominating mechanism which impedes the flow through the pores. The classical description of flow through mud is therefore one in which the pressure gradient is balanced by friction. Because of the complexity of the sand skeleton this is necessarily an empirical relation, known as Darcy's law (e.g. Sleath 1984):

$$\mathbf{u} = -k\nabla p,$$

where $\mathbf{u} = (u,v,w)$ is the fluid velocity in direction $x = (x,y,z)$-respectively, z pointing upwards, against gravity, p is the pressure, $\nabla = \partial/\partial x, \partial/\partial y, \partial/\partial z$ the gradient operator, and k an empirical constant proportional to the mud's permeability (proportional to the porosity of the mud), and inversely proportional to the viscosity of water. Although the pores may contain a substantial amount of air, which will make the aggregate of air and water within the pores susceptible to compression, we adopt the simplistic viewpoint that the pores are entirely filled with water, which is (nearly) incompressible. Hence the fluid is non-divergent:

$$\nabla \cdot \mathbf{u} = 0$$

(Accounting for the slight compressibility of water, or of the water-air mixture, would enable us to describe acoustic waves. For the range of probing frequencies given, however, these waves would have length scales of some hundreds of meters, far outside the range of interest of 5 cm, say.) Incompressibility of the pore water (adopted here) means that pressure variations will instantaneously be felt throughout this domain of interest. The probing bill will bodily displace sand and water and thus will also act as a mass source. This is modelled by introducing a source term at the right-hand side of the last equation. In the approximation that this is a point-source this will take the character of a Dirac delta function $\delta(\mathbf{x})$, a 'distribution', whose integral value only has physical significance representing the mass flux.

Role of repetitive probing

Assuming the permeability k to be spatially uniform, the previous two equations, with the addition of a point source, can be combined into a Poisson equation for the pressure:

$$\Delta p = \delta(\mathbf{x})\, e^{2\pi i f t} \qquad (1)$$

where the Laplacian operator $\Delta = d^2/dx^2 + d^2/dy^2 + d^2/dz^2$. Note that this only determines a spatial relationship for the pressure. Its time (t) dependence (introduced by the repetitive probing with frequency f) is parametric: $p \propto exp(2\pi i f t)$. Omitting the time-dependence (see below) the Poisson equation, (1), is solved by $p = 1/r$, where $r = (x^2 + y^2 + z^2)^{1/2}$ represents radial distance. The pressure in an infinite medium (for the

moment disregarding the upper surface), is thus simply inversely proportional to the distance to the source.

The knot's 'sixth sense' for remote detection of prey (Piersma et al 1998), employing repetitive, shallow probing, followed by a single deep probe in another direction, apparently uses the *build-up* of residual pressure near the knot's bill tip. Compaction may be responsible for such pressure build up. The periodic `shaking' of muddy sand by the probing action of the bill may explain the continuous increase in residual pore pressure. Each shake may lead to a (locally) more compact rearrangement of sand grains when the stirred-up sand grains fall back under the action of gravity. This process may lead to an associated increase of pore pressure and plays a dominant role, for example in liquefaction and the formation of quick sand (Sleath 1984). But the pressure field is not only changing in the vicinity of the bill. The residual (time-averaged) pressure pattern in the vicinity of a nearby shell will be affected as well, and in consequence this will in turn affect the pressure distribution around the bill. The intensity of this spatially-modified pressure pattern will increase at each successive cycle of the probing action, revealing the prey's location by making it, in every cycle more clearly 'visible'.

Response due to a rhizome layer with or without a shell

At the top of the rhizomes layer, situated at depth $z = -d$, the pressure, p, and the vertical velocity, $w = -kdp/dz$, perpendicular to that plane, have to be continuous. The permeability, k, of the lower rhizomes layer, k_l, is less than that of the upper mud layer, k_u. This is due to the decrease in the effective porosity of the sediment, and we assume that the rhizome root structure is so small that we can represent its presence in the form of a reduced effective permeability.

We next describe the response due to a localized pressure pulse induced by repetitive probing of a knot's bill, at $z = 0$. We consider three cases: first, the response in the absence of a shell, when a mud layer rests on top of a layer containing a rhizomes mat: second, the response to a shell in a mud layer without a rhizome mat, qualitatively discussed in Piersma et al (1998): third, the response to a shell buried in the lower layer containing the rhizomes mat. In the latter case we give particular attention to the pressure gradient sensed at the position of the knot's bill.

Response due to a rhizomes layer without a shell

Even in the absence of a prey (or stone) the change in permeability between a mud layer and a layer containing a seagrass root system (rhizomes mat) will affect the radial pressure distribution discussed above. Assuming the permeability to be constant within the rhizome layer, the pressure will again be governed by a Laplace equation. Hence the pressure will also be inversely proportional the radius, but with a reduced 'transmitted' amplitude T. The semipermeable interface between the mud and rhizome layers acts as a partial mirror. Therefore it augments the pressure field in the mud layer, where the knot senses the pressure difference relative to the uninhibited pressure field it knows it has been producing. This augmented field in the mud layer seems to come from a mirror

source situated in the rhizome layer at a distance from the interface at $z = -d$ equal to that of the source (the bill), at the surface and the interface. Therefore, the pressure is written as

$$p(x,y,z) = \begin{cases} p_u = \dfrac{1}{r_0} + \dfrac{R}{r_{-1}}, & z \in (-d, 0) \\ p_l = \dfrac{T}{r_0}, & z < -d \end{cases} \tag{2}$$

where $r_n \equiv (x^2 + y^2 + (z + Z_n)^2)^{1/2}$, denotes the distance with respect to source ($n = 0$) or images, located at $Z_n = -2nd$ for $n = (1,2,\ldots)$. At the interface between mud and rhizome layer, $z = -d$, we require continuity of the pressure $p_u = p_l$, (subscripts denoting upper (u) and lower (l) layer respectively), and also continuity of vertical velocity $k_u\, dp_u/d_z = k_l\, dp_l/d_l$. This determines reflection and transmission coefficients R and T in terms of $k = k_l/k_u < 1$:

$$R = \frac{1-k}{1+k}, \quad T = \frac{2}{1+k}. \tag{3}$$

The resulting pressure field is displayed in Fig. B6.1A.
In this computation, the top layer ($z > -d$) is treated as being of infinite extent. Therefore, the normal derivative of the pressure, dp/dz, and hence the vertical velocity, w, do not vanish at the water surface, $z = 0$. Figure B6.1A shows a weak inclination of the isobars relative to the vertical. The presence of the water surface, however, leads to a subsequent reflection of our virtual source at $z = -2d$, which creates a new mirror image above the water surface, at $z = 2d$. This mirror source, in turn, will produce a subsequent mirror source in the rhizomes layer at $z = -4d$ and so on, *ad infinitum*, and the pressure field due to this infinite sequence of source and mirror images is given by

$$p(x,y,z) = \begin{cases} p_u = \sum_{n=0}^{\infty} \left(\dfrac{R^n}{r_n} + \dfrac{R^{n+1}}{r_{-(n+1)}} \right), & z \in (-d, 0) \\ p_l = T \sum_{n=0}^{\infty} \dfrac{R^n}{r_n}, & z < -d \end{cases} \tag{4}$$

Taking for example, 50 mirror sources into account, the isobars indeed approach the water surface practically orthogonally (see Fig. B6.1B). When we subtract the initial pulse, we find the pressure perturbation as sensed by the knot (Fig. B.6.1C), which the knot may take to indicate the presence of a prey straight below its bill.

Perturbation due to a spherical shell

We now consider the impact of a shell (Piersma et al. 1998). For convenience this is assumed to be of spherical shape or radiusa <1, located at a radial distance $r = 1$ from the bill tip, at an oblique angle θ from the horizontal. In an infinitely extended mud layer, an appropriate array of image sources and sinks, located within the shell, will be able to generate a pressure and corresponding motion field such that the isobars are

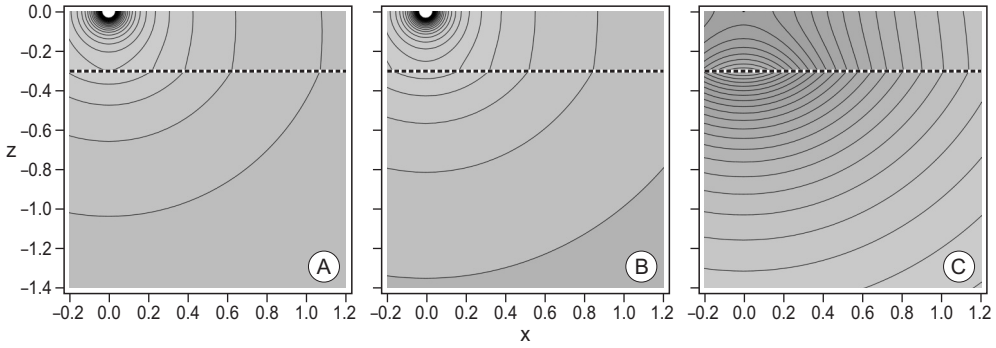

Figure B6.1 Rhizomes layer *without* shell: Pressure distribution, $p(\mathbf{x},z)$, for $k = 0.25$ taking in the summation (A) only the $n = 0$ term into account, or (B) up to $n = 50$. The top of the rhizomes layer is indicated by a dashed line. (C) Pressure perturbation, $p'(x,z) \equiv p - 1$, after eliminating the forced pulse at the source.

everywhere perpendicular, and thus the flow is parallel to the shell's boundary (Lamb 1932; p. 129), Fig. B6.2A. We let the source be at the origin and the centre of the shell define the x,z-plane. The residual pressure field is then most easily expressed in a coordinate system in which the x,z-coordinates, rotated to ξ,ζ-coordinates, with $\xi = -xs + zc$, $\zeta = xc + zs$, and $(s,c) \equiv (\sin\theta, \cos\theta)$, are such that the line connecting bill tip and prey is now defined as the new horizontal ξ-axis, and the line perpendicular to this as the new vertical ζ-axis. Then the residual pressure reads

$$p(x,y,z) = \frac{1}{r} + \frac{a}{\sqrt{(1-a^2-\zeta)^2+\rho^2}} + \frac{1}{a}\left[sinh^{-1}\left(\frac{1-a^2-\zeta}{\rho}\right) - sinh^{-1}\left(\frac{1-\zeta}{\rho}\right)\right],$$

where $\rho = (\xi^2 + y^2)^{1/2}$ is a horizontal radial coordinate. Subsequent figures show the $y = 0$ plane only (the plane containing bill tip and prey), in which the response is strongest. When we subtract the initial pulse, we find, however, that the isobars of the perturbation pressure field are not perpendicular to the water surface, $z = 0$, suggesting a flow through the surface (Fig. B6.2B) but this does not happen since the water surface is impenetrable. The surface acts as a reflector leading to another change in the pressure field. This is produced by a mirror image of the virtual sources invoked by the shell. Adding this contribution, the isobars are correctly perpendicular to the water surface (Fig. B6.2C) but at the bill tip, at the origin, $(x,z) = (0,0)$, this difference is sensed and informs the knot about the presence of a prey at $\theta = 60°$ relative to the horizontal, at a radial distance $r = 1$. Note that these image sources (located *above* the water surface) would require another perturbation pressure field in the vicinity of the shell, as the flow induced by that field would equally need to avoid penetrating the shell. In theory, an infinite sequence of virtual sources within the shell and above the water surface would be needed to exactly satisfy the impenetrability at shell and water surfaces. In practice, here and in what follows, we truncate this sequence after a few terms. When the shell is buried in a half-infinite

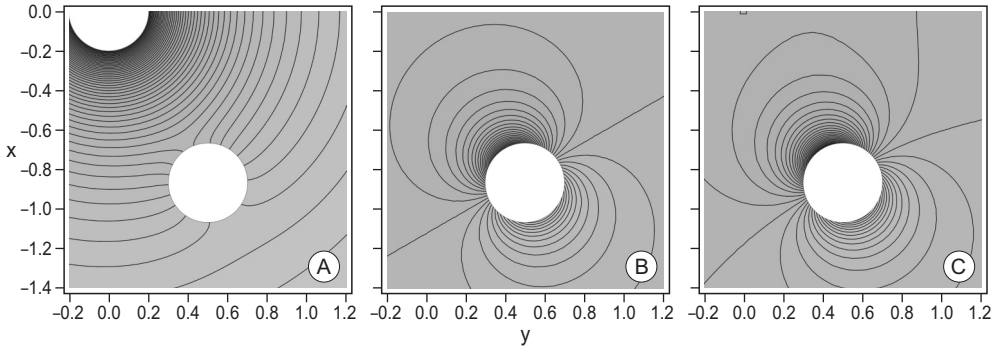

Figure B6.2 Shell without rhizomes layer: (A) Pressure distribution, $p(X,z)$, due to shell in infinitely deep mud layer without rhizomes. (B) Perturbation pressure, $p'(X,z)$ without the source. (C) As (B), but with reflecting water surface.

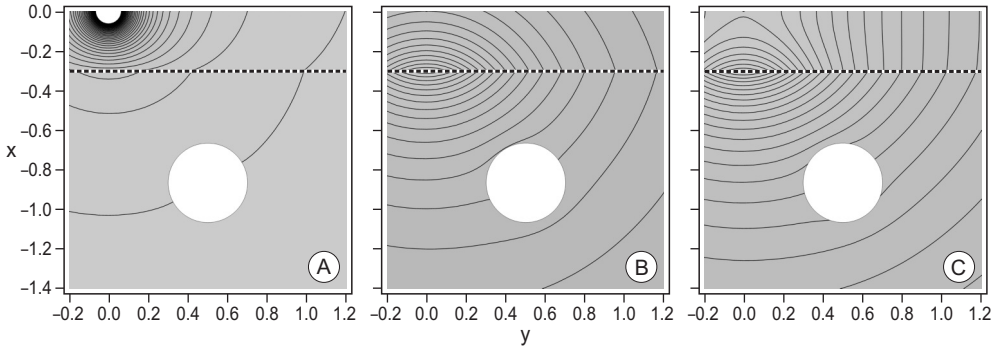

Figure B6.3 Shell within a rhizomes layer: (A) Pressure distribution , $p(X,z)$, due to shell in infinitely deep rhizomes layer located below mud layer. The interface between both layers is indicated by a dashed line. (B) Perturbation pressure $p'(X,z)$ without the source. (C) As (C), but with reflecting water surface.

rhizome layer of permeability $k = 0.25$ (leading to a reflection coefficient, $R = 0.6$) below a mud layer of depth $d = 0.3$, the rhizome mat changes the apparent strength of the source at the origin by a factor $T = 1 - R^2$. The change in the pressure field at the interface between mud and rhizome layer is clearly visible in a changing isobar inclination (Fig. B6.3A). Subtracting the influence of the source (Fig. B6.3B) shows that the pressure field in the mud layer no longer reveals the presence of the shell, even if we take the mirroring aspect of the surface into account (Fig. B6.3C). In both cases, the pressure difference is very nearly symmetric at the bill tip, at the origin $x = 0$, and no longer offers any clues on the direction (or distance) at which the prey can be found (compare Fig. B6.3C with Fig. B6.2C). In fact, while not *exactly* symmetric, it is clear that the pressure difference $p' = p - r^{-1}$ between the induced (p), and the imposed pressure r^{-1} – the difference sensed by the knot – is dominated by the direct reflection due to the presence of the

rhizome layer. This overwhelms the much weaker pressure difference due to the reflection by the shell and obscures the directional prey information.

Perturbation pressure gradient

The pressure difference below the top layer of depth d, of course, also depends on the actual change in permeability, k, due to a rhizome mat below, on shell size, a, and on shell angle, θ, relative to the horizontal. (We here assume the rhizome mat to be of semi-infinite extent). The strength of the pressure gradient as sensed by the knot's bill is estimated by taking only the influence of the rhizome layer and of a shell into account. Thus we discard the subsequent contribution consisting of mirror images due to the presence of the surface. The reason to do so is that the vertical component of the pressure gradient (proportional to the vertical velocity) vanishes at the surface. Since the knot's bill penetrates the mud layer over a few millimetres, the knot also senses this difference below the surface, where this component is not annihilated. In this way, the pressure gradient at the origin, $(x,y) = (0,0)$, affected by the sea grass roots and a shell, contains apart from its magnitude, directional information, ϕ, which can be computed analytically. It is given by

$$-\nabla p' \equiv |\nabla p'|(\cos\phi, \sin\phi) = (1-R^2)\frac{a^3}{(1-a^2)^2}(\cos\theta, \sin\theta) + \left(0, \frac{R}{4d^2}\right).$$

Without a rhizome layer, the permeability ratio $k = 1$, and thus there is no reflection, $R = 0$, and the pressure gradient decreases with decreasing shell size, a. In the vertical plane this points towards the shell position, $\phi = \theta$. With a rhizome layer, but *without* a shell ($a = 0$), the perturbation pressure gradient points simply downwards, towards the image source. This may falsely suggest the presence of a shell at a depth $2d$, twice the thickness of the sediment layer on top. For a single depth $d = 0.3$ and shell diameter $a = 0.2$, the

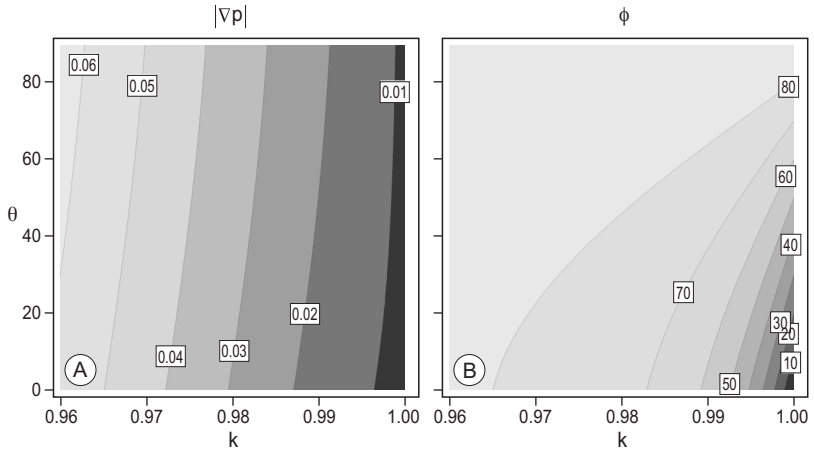

Figure B6.4 Perturbation pressure gradient sensed at the bill tip ($x = (0,0,0)$): (A) magnitude, $|\nabla p|$, (dimensionless units and colours) and (B) direction, ϕ, (labelled contours in degrees and colour) as a function of shell angle to the horizontal, θ, and of permeability ratio, k.

magnitude $|\nabla p'|$ and direction ϕ, relative to the horizontal, are displayed in Figures B6.4A, B. The figure reveals that even under a small 4% drop of permeability in the lower rhizomes layer, the perturbation pressure gradient magnitude increases by a factor of 10 (see the left side of Fig. B6.4A). Obviously, the contribution to the perturbation pressure by the shell is dwarfed by that due to the virtual image source. Most significantly, the angular information on the position of the shell is almost lost, since $\phi \approx 90^\circ$ for any shell direction θ (meaning the knot believes the prey to be buried vertically below the bill). This sensitive dependence on permeability remains present for other surface layer depths, d, and shell diameters, a.